# PHOTONICS Research

# Single optical microfiber enabled tactile sensor for simultaneous temperature and pressure measurement

Ni Yao,[1,†] Xiaoyu Wang,[1,†] Shuqi Ma,[1,†] Xingda Song,[2] Shan Wang,[1] Zhangxing Shi,[3] Jing Pan,[2] Shipeng Wang,[1] Jianliang Xiao,[1] Haitao Liu,[1] Longteng Yu,[1] Yao Tang,[2] Zhang Zhang,[2] Xiong Li,[4] Wei Fang,[2,5] Lei Zhang,[1,2,6] and Limin Tong[1]

[1]*Research Center for Humanoid Sensing, Zhejiang Lab, Hangzhou 311121, China*
[2]*State Key Laboratory of Modern Optical Instrumentation, College of Optical Science and Engineering, Zhejiang University, Hangzhou 310027, China*
[3]*Shandong Institute of Advanced Technology, Jinan 250100, China*
[4]*Tencent Robotics X Lab, Tencent Technology (Shenzhen) Co., Ltd, Shenzhen 518054, China*
[5]*e-mail: wfang08@zju.edu.cn*
[6]*e-mail: zhang_lei@zju.edu.cn*

The ability to sense heat and touch is essential for healthcare, robotics, and human–machine interfaces. By taking advantage of the engineerable waveguiding properties, we design and fabricate a flexible optical microfiber sensor for simultaneous temperature and pressure measurement based on theoretical calculation. The sensor exhibits a high temperature sensitivity of 1.2 nm/°C by measuring the shift of a high-order mode cutoff wavelength in the short-wavelength range. In the case of pressure sensing, the sensor shows a sensitivity of 4.5% per kilopascal with a fast temporal frequency response of 1000 Hz owing to the strong evanescent wave guided outside the microfiber. The cross talk is negligible because the temperature and pressure signals are measured at different wavelengths based on different mechanisms. The properties of fast temporal response, high temperature, and pressure sensitivity enable the sensor for real-time skin temperature and wrist pulse measurements, which is critical to the accurate analysis of pulse waveforms. We believe the sensor will have great potential in wearable optical devices ranging from healthcare to humanoid robots. © 2022 Chinese Laser Press

https://doi.org/10.1364/PRJ.461182

## 1. INTRODUCTION

The ability to sense heat, cold, and touch is essential for the human being to survive and interact with the world. As a counterpart of our skin, skin-like tactile sensors with temperature and pressure sensing abilities [1–3] play an essential role in next-generation healthcare [4–6], robotics [7,8], and human–machine interfaces [9,10]. Recently, the rapid development of electronic tactile sensors [11–15] triggered the research of optical tactile sensors due to their attractive advantages, such as high sensitivity, fast response, and immunity to electromagnetic interference [16]. For example, Zhao *et al.* reported stretchable optical waveguides (3 mm in diameter) for strain sensing in a prosthetic hand [17]. Wang *et al.* developed a fiber optic mattress for noninvasive monitoring of vital signs based on a silica optical fiber (0.125 mm in diameter) Mach–Zehnder interferometer [18]. Guo *et al.* demonstrated an optical sensor that can simultaneously detect and distinguish temperature and strain using a polydimethylsiloxane (PDMS) fiber (0.5 mm in diameter) doped with upconversion nanoparticles [19]. Although some fiber

optic sensors have demonstrated dual/multiple sensing abilities [20–24], it is difficult to assemble a compact wearable sensor using silica optical fibers or the above-mentioned polymer fibers for healthcare or robotic applications due to the lack of flexibility, large size, or expensive signal processing instruments.

Optical microfibers, with diameters close to or below the wavelength of visible or near-infrared light, offer widely tailorable optical confinement and evanescent fields, which is very attractive to optical sensing on the micrometer and nanometer scales [25–27]. To date, optical microfiber tactile sensors have been attracting increasing research interest due to their possibilities of realizing miniaturized fiber optic sensors with a small footprint, high sensitivity, fast response, high flexibility, and low optical power consumption [28–31]. In our previous works, highly sensitive temperature [32] and pressure [33,34] sensors were developed by embedding microfiber into a thin layer of PDMS film. Because temperature and pressure stimuli often mix together, it is challenging to detect temperature and pressure simultaneously by simply recording the output optical intensity.

In this work, we demonstrate a single optical microfiber enabled tactile sensor for simultaneous temperature and pressure measurement. Typically, a biconical tapered microfiber with a specially designed diameter (e.g., 2.0 μm) is fabricated and embedded in a thin layer of PDMS film based on theoretical simulation. For temperature sensing, shifting a high-order mode cutoff wavelength in a short-wavelength region (e.g., 510–610 nm) is used, as the refractive index of the PDMS layer that determines the cutoff wavelength of the high-order mode is a function of temperature, while the spectrum in the long-wavelength region (e.g., 700–1000 nm) shows a negligible change. When exerting external pressure on the sensor, the peak wavelength representing the high-order mode cutoff has no change, but the pressure caused bending loss leads to a significant output intensity change in the long-wavelength region. Thus, the cross-talk issue can be addressed by choosing two wavelength regions for temperature and pressure measurement. The sensor demonstrates high sensitivity, fast temporal response, and excellent reversibility. As a proof of concept, highly sensitive wrist pulse together with skin temperature measurement is realized, which is critical to the accurate analysis of pulse waveforms.

## 2. CONCEPTS, STRUCTURES, AND SENSING PRINCIPLE

Human skin has different types of tactile receptors (e.g., Ruffini ending, Pacinian corpuscles, and free nerve ending) that can feel mechanical and temperature stimuli [35–37]. In contrast to electrical multiple-parameter tactile sensors integrating individual sensing elements [11], optical sensors offer more options

for signal retrieval from optical intensity, spectrum, phase, and polarization [38]. Mimicking the tactile sensing function of human skin, a single microfiber enabled optical sensor that can simultaneously detect and distinguish temperature and pressure is developed by taking advantage of microfiber's engineerable optical properties, as shown in Fig. 1(a). Briefly, we choose PDMS to embed a biconical tapered silica microfiber due to its low refractive index (~1.40 of PDMS versus ~1.46 of silica), large thermo-optic coefficient (–10$^{-4}$ °C$^{-1}$) [39], low Young's modulus ($E_P = 750$ kPa), and biocompatibility. The flexible PDMS film does not only convert temperature stimuli into the change of refractive index contrast, resulting in a cutoff wavelength shift of a particular high-order mode, as shown in Fig. 1(b), but also transduces pressure stimuli into deformation of the microfiber with high fidelity, leading to a bending-induced drop in output intensity, as demonstrated in Fig. 1(c). By optimizing the diameter of the microfiber, it is possible to choose two wavelengths to realize simultaneous temperature and pressure sensing with negligible cross talk. Experimentally, the excellent mechanical property, the high flexibility, and conformal attachment capability, as shown in Fig. 1(d), Fig. 1(e), and Fig. 1(f), respectively, make the sensor suitable for skin physiological monitoring and robotics applications.

## 3. THEORETICAL CALCULATION

The waveguiding modes supported by microfiber can be characterized by normalized propagation constant $V = 2\pi a \sqrt{n_1^2 - n_2^2}/\lambda$, where $\lambda$ is the propagation wavelength, $a$ is the radius of the microfiber, $n_1$ and $n_2$ are the refractive index
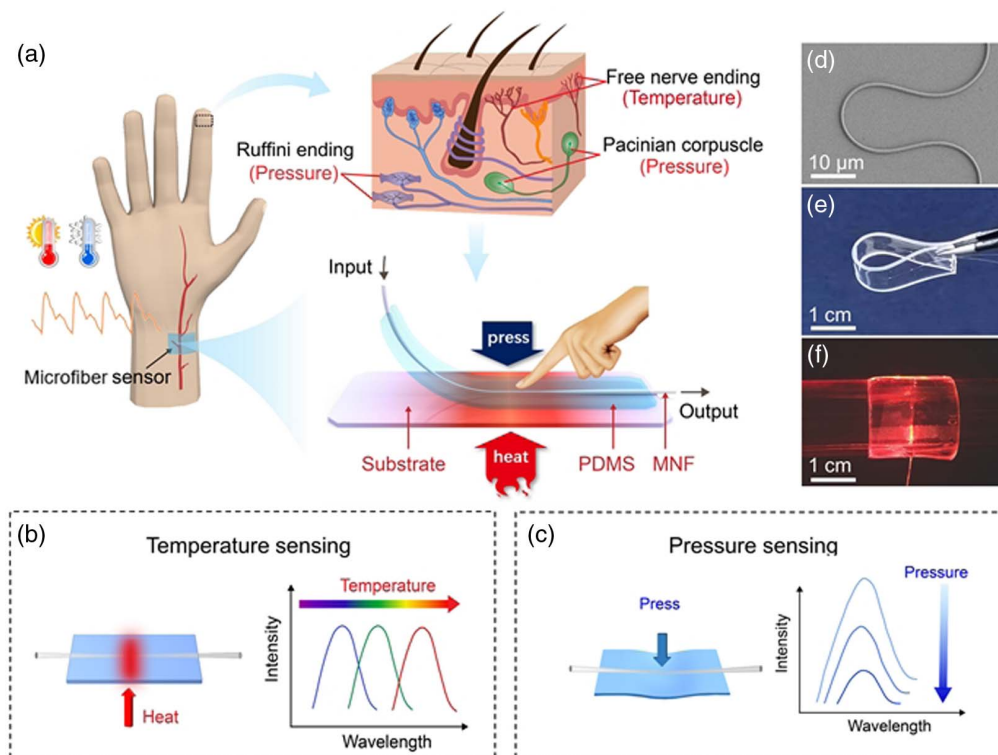


**Fig. 1.** Single optical microfiber enabled tactile sensor for simultaneous temperature and pressure sensing. (a) Schematic of the human skin inspired microfiber sensor. Schematic illustration of the (b) temperature and (c) pressure sensing mechanism. (d) SEM image of a bent microfiber. (e) Photograph of a flexible bending sensor. (f) Photograph of a sensor attached to a glass vial.

of the core and cladding of microfiber, respectively. The core and cladding layers of the microfiber sensors are formed by silica and PDMS, respectively. When the temperature increases, the refractive index of PDMS decreases much faster than that of silica as it has a large thermo-optic coefficient ($-10^{-4}$ °C$^{-1}$). The increase in refractive index contrast results in a redshift of the cutoff wavelength of a particular high-order mode. Thus, the supported high-order modes depend entirely on temperature, the radius of the microfiber, and the propagation wavelength. To achieve the temperature measurement in a desired wavelength range, precise control of the microfiber diameter is needed. Typically, diameter-dependent mode effective refractive indices of microfiber packaged by PDMS at the wavelength of 532 nm are shown in Fig. 2(a), where the refractive indices of the core silica and cladding PDMS are 1.461 and 1.397, respectively, at 25°C. The microfiber diameter is chosen as 2 μm because the high-order $EH_{21}$ mode can be easily excited. Thus, the cutoff of this mode will introduce an abrupt intensity change in the transmission spectrum.

## 4. EXPERIMENTAL SECTION

### A. Fabrication of Dual-Parameter Optical Microfiber-Based Sensor

The microfiber used in the device is tapered from a multimode fiber (SX62.5, Corning) by a home-built fiber-puller system that consists of a hydrogen flame torch, two motorized translation stages, and optical measurement components. During the pulling process, a continuous-wave laser at 785 nm is coupled into the multimode fiber to excite certain high-order modes. From the cutoff of high-order modes (transmission

intensity abrupt drops), microfiber with a desired diameter can be precisely fabricated. The target diameter of the microfiber is set at 2 μm so that only one high-order $EH_{21}$ mode is terminated around the wavelength of 532 nm, and the interference between degenerate modes is avoided, as shown in Fig. 2(a). Once the microfiber is fabricated, it is placed on a 300 μm thick PDMS film and then covered by another layer of degassed PDMS to form a film with a total thickness of 600 μm. The whole structure is then cured at 80°C for 15 min.

### B. Experimental Setup for Temperature and Pressure Sensing

Broadband light from a tungsten halide lamp (SLS201L, Thorlabs) is coupled into the sensor. The transmitted light is recorded by a spectrometer (Maya2000 Pro, Ocean Optics). The sensor is placed on a hot plate (IKA-Ret Basic) for temperature control. A tip integrated with force gauge is mounted on a three-dimensional translation stage with differential actuators for fine pressure adjustment.

## 5. RESULTS AND DISCUSSIONS

To investigate the temperature sensing performance, the sensor is put on a hot plate with a controlled temperature ranging from 25°C to 95°C, and the transmitted spectra are recorded by a spectrometer. Figure 2(b) gives transmission spectra recorded at different temperatures when the diameter of the microfiber is chosen as 2 μm. We find that the peak corresponding to the cutoff wavelength of a higher-order mode shows an obvious redshift, while the spectra have no change in the long-wavelength range (e.g., 700–1000 nm). To verify that this
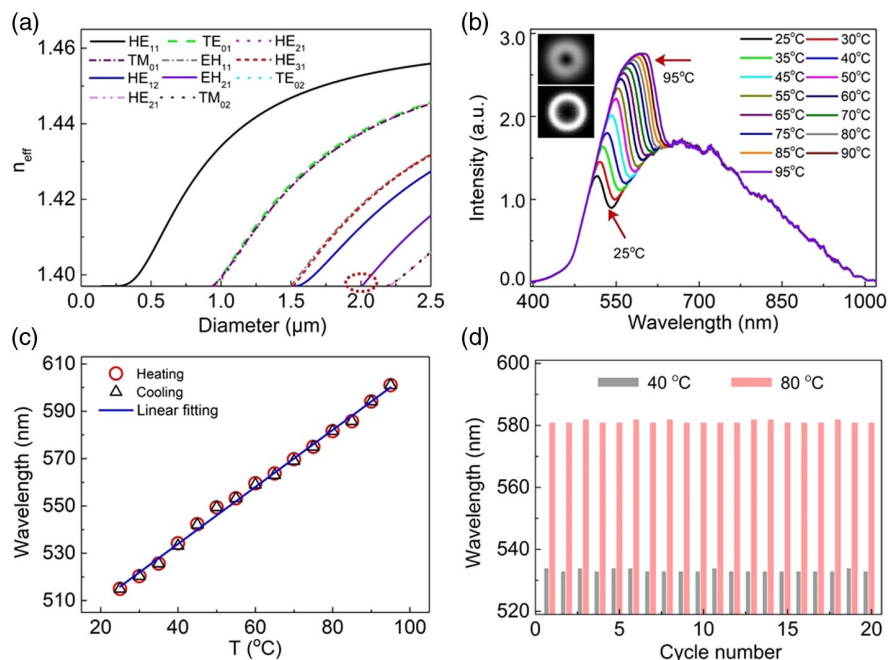


**Fig. 2.** Temperature responses of the sensor. (a) The effective refractive indices of supported modes as functions of microfiber diameter at 532 nm wavelength. (b) Transmission spectra at different temperatures. The upper inset and the lower inset show the measured higher-order mode intensity profile and calculated $EH_{21}$ mode intensity profile, respectively. (c) Peak wavelength of $EH_{21}$ mode as a function of temperature. The red circles and black triangles represent the heating and cooling process, respectively. *T*, temperature. (d) Repeatability of the sensor is tested by alternately switching the temperature between 40°C and 80°C.
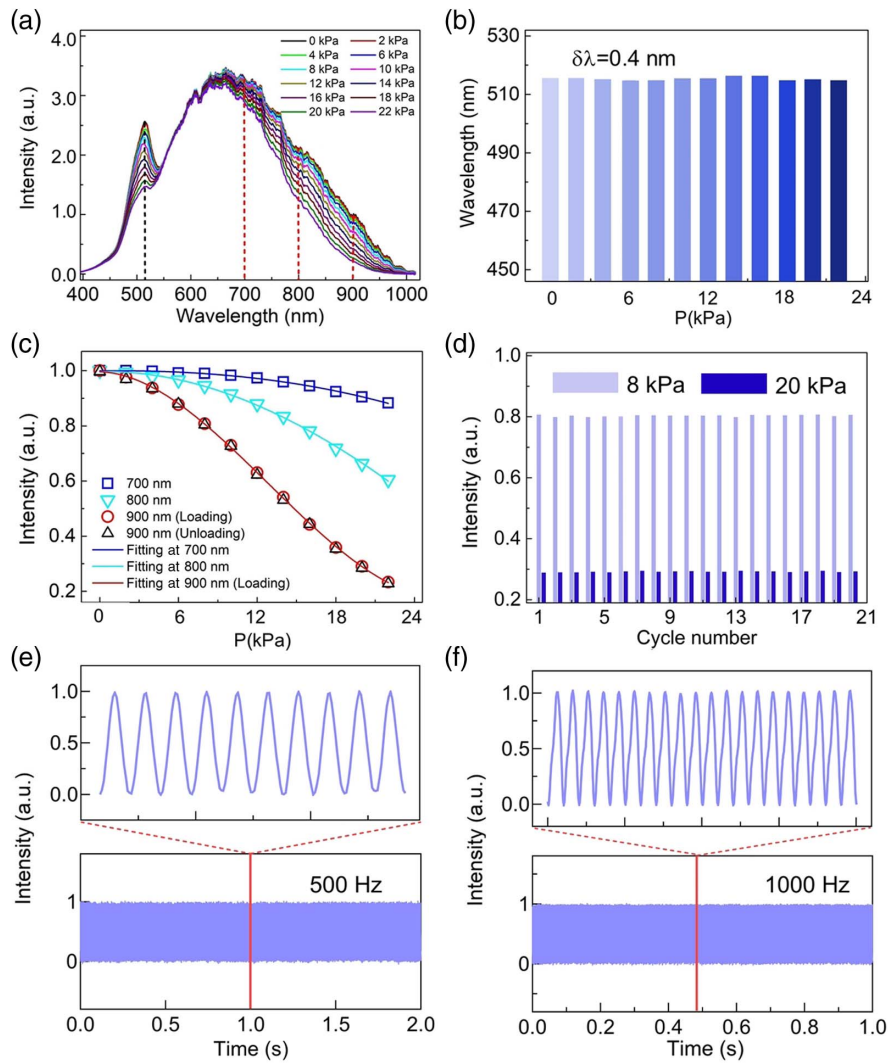
**Fig. 3.** Pressure responses of the sensor. (a) Transmission spectra under various pressures. (b) The peak wavelength corresponding to the cutoff of high-order $EH_{21}$ mode under various pressures. The standard deviation of the wavelength distribution is 0.4 nm. (c) The normalized intensities at 700 nm, 800 nm, and 900 nm, respectively, as functions of pressures. (d) Repeatability of the sensor to static pressure. The sensor response to dynamic pressure at (e) 500 Hz and (f) 1000 Hz, respectively.

higher-order mode is indeed the $EH_{21}$ mode as predicted in Fig. 2(a), the output intensity profiles of the fiber are measured after passing through a 600 nm short-pass filter and a 550 nm long-pass filter. Subtracting the profile at 25°C from the one at 95°C results in a donut-shaped intensity distribution, which coincides with the simulated profile of the $EH_{21}$ mode, as shown in the insets of Fig. 2(b). As shown in Fig. 2(c), the data derived from Fig. 2(b) are fitted by $\lambda = 485.5 + 1.205T$, which results in a temperature sensitivity as $S = \Delta\lambda/\Delta T = 1.205$ nm/°C, where $\lambda$, $T$, $\Delta\lambda$, and $\Delta T$ are peak wavelength, temperature, the shift of peak wavelength, and the change of temperature, respectively. To test its reversibility, the sensor is tested by alternatively changing the temperature of the hot plate from 40°C to 80°C. After 20 circles, the shift of peak wavelengths shows excellent repeatability demonstrated in Fig. 2(d), indicating the reliability of the sensor for potential applications in health monitoring and robotics.

To measure the responses of the sensor to static pressure, a motorized force tester equipped with a digital force gauge is used to provide an external pressure. Figure 3(a) plots the spectra recorded at different pressures controlled by the force tester. The output intensity experiences a gradual decrease in the wavelength range from 700 nm to 1000 nm with the external pressure varying from 0 kPa to 22 kPa. We find that the peak intensity at 515 nm shows a noticeable decrease, while the peak wavelength corresponding to the cutoff of the high-order $EH_{21}$ mode has negligible change, as demonstrated in Fig. 3(b). Figure 3(c) shows that the pressure sensitivity increases with the increase of the wavelength from 700 nm to 900 nm, as a result of the increasing fractional evanescent fields. For the wavelength of 900 nm, the intensity shows a nearly linear response to the pressure in a range of 6 kPa to 20 kPa, achieving a sensitivity of 4.5%/kPa by defining sensitivity as $S = \Delta I/\Delta P$ derived by $I = 0.9961 - 1.610 \times 10^{-3}P - 3.480 \times 10^{-3}P^2 + 8.968 \times 10^{-5}P^3$,

**Table 1.  Comparison between Experimental Setting Values and Measurement Results**

| | Experimental Setting | | Measurement Result | | Error | |
|---|---|---|---|---|---|---|
| | $T$ (°C) | $P$ (kPa) | $T$ (°C) | $P$ (kPa) | $T$ | $P$ |
| 1 | 29 | 4.04 | 28.8 | 4.12 | 0.67% | 1.94% |
| 2 | 30 | 15.96 | 30.1 | 16.10 | 0.33% | 0.87% |
| 3 | 46 | 10.06 | 45.8 | 10.24 | 0.44% | 0.90% |
| 4 | 59 | 3.94 | 58.5 | 4.04 | 0.85% | 1.50% |
| 5 | 60 | 15.90 | 60.3 | 16.04 | 0.50% | 0.88% |

where $I$, $P$, $\Delta I$, and $\Delta P$ are the normalized intensity, pressure, the change of normalized intensity, and the change of the pressure, respectively. The coincidence of data points between loading and unloading processes verifies the reliability of the sensor. The sensor also exhibits excellent stability by alternatively changing from 8 kPa to 20 kPa for 20 circles, as shown in Fig. 3(d). Benefiting from the robust encapsulation of the microfiber in the PDMS, no noticeable performance degradation is observed.

To test the response of our sensor to dynamic pressure, a home-built vibration test platform that consists of a vibration actuator, a power amplifier, and an oscilloscope is used to record the output signals. As shown in Figs. 3(e) and 3(f), the clear distinguishability up to 1000 Hz and excellent reversibility of the peak intensity over 1000 cycles indicate a fast temporal response and long-term stability, offering a possibility for

real-time monitoring of pressure-related signals, e.g., wrist pulse with high accuracy.

To illustrate simultaneous temperature and pressure sensing, we carry out a series of measurements at different temperature and pressure conditions. The experimental results are shown in Table 1, where $T$ and $P$ are temperature and pressure, respectively. Here the measured pressure values are directly interpolated from the fitting curve at 900 nm shown in Fig. 3(c). The overall error resulted from single parameter fitting as <1% for temperature measurement and <2% for pressure measurement, respectively, indicating the sensor based on such a simple structure can measure temperature and pressure simultaneously with negligible cross talk.

The artery pulse waveform monitoring is a safe, noninvasive means of performing the cardiovascular problem analysis [40], while the skin temperature variation will influence the artery pulse waveforms because heat and cold changes affect the blood vessels vasodilation and vasoconstriction, respectively [41]. Therefore, to realize an accurate analysis of pulse waveforms, it is necessary to measure temperature together with pulse monitoring. Here we demonstrate simultaneous skin temperature and wrist pulse monitoring capabilities by attaching our sensor to a healthy volunteer's wrist, as shown in Fig. 4(a). The inset of Fig. 4(a) demonstrates the blood vessel undergoes vasoconstriction and vasodilation under cold and warm conditions. Obviously, the cold conditions will result in blood vessel vasoconstriction, and vice versa. The sensor can readily read out wrist pulse difference before and after exercise by utilizing the
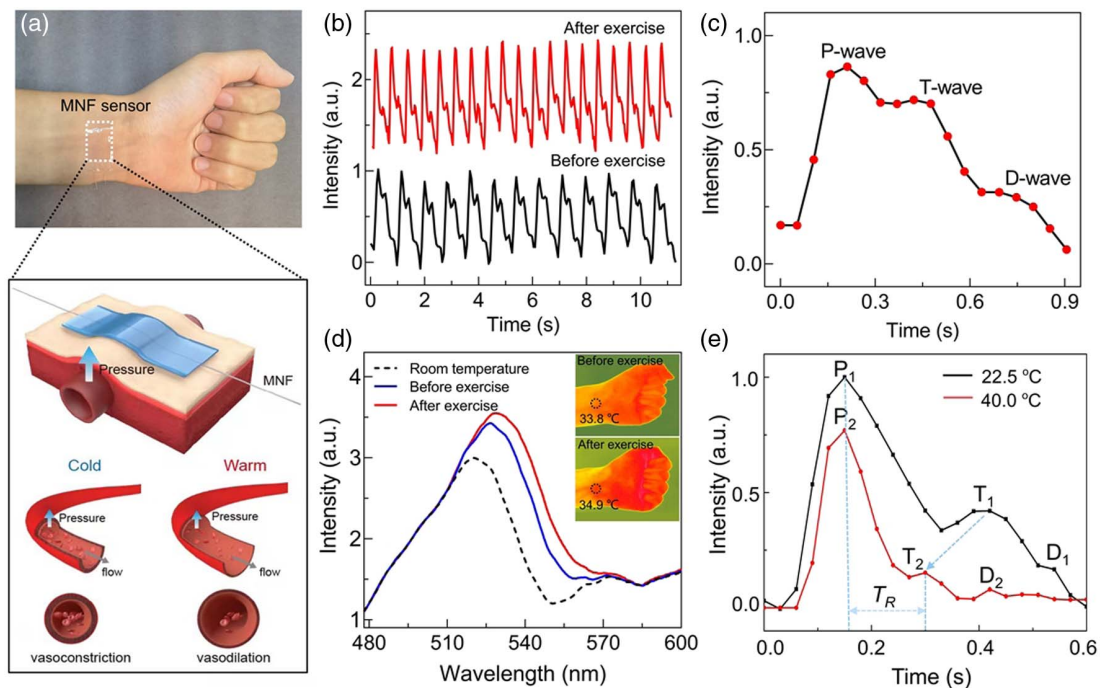


**Fig. 4.** Simultaneous monitoring of temperature and the wrist pulse. (a) Photograph showing a single microfiber sensor for skin temperature and wrist pulse sensing, and the enlarged schematic diagram indicates the effect of temperature on the constriction and dilation of arterial vessels. (b) Wrist pulse waveform before and after exercise. (c) Typical wrist pulse waveform with measured distinguishable P-wave, T-wave, and D-wave peaks. (d) Typical spectral response of a microfiber sensor device directly above the artery of the wrist at room temperature, before and after exercise, and the infrared thermal image showing the temperature distribution of the wrist before and after exercise. (e) Comparison of the artery pulse pressure waveform variation with wrist temperature of 22.5°C and 40.0°C.

pressure sensing function, and the wrist pulses before and after exercise are 69 beats/min and 101 beats/min, respectively, as illustrated in Fig. 4(b). The three typical peaks, such as the percussion wave (P-wave), tidal wave (T-wave), and diastolic wave (D-wave), are clearly visible, as shown in Fig. 4(c). Figure 4(d) describes the sensor's temperature response before and after exercise. The measured transmission peak presents a 1.3 nm wavelength redshift after exercise, corresponding to a temperature change of 1.1°C. For comparison, the thermal images obtained by an infrared camera show 1.1°C temperature change in wrist via exercise, as demonstrated in the inset of Fig. 4(d), exhibiting its consistency with the spectral response curve. In addition, the artery pulse pressure illustrates the different waveforms at cold (22.5°C) and warm (40.0°C) conditions, and the round-trip time ($T_R$) decreases with an increase of the temperature, as shown in Fig. 4(e). The sensor with temperature and pressure sensing capabilities shows its great application potential in healthcare.

## 6. SUMMARY

In summary, a simple optical microfiber tactile sensor is designed and fabricated for simultaneous detection of temperature and pressure by tailoring the waveguiding properties. Typically, an optical microfiber with 2 μm diameter is embedded into a thin film of PDMS to sense the thermal and mechanical stimuli. In this case, the shift of a high-order mode cutoff wavelength in the short-wavelength range is employed for temperature measurement, while the intensity change in the long-wavelength range is used for pressure sensing. Benefiting from the high thermo-optic coefficient of PDMS and considerable fractional power guided outside the microfiber, the sensor achieves high sensitivity in both temperature and pressure sensing. Furthermore, the sensor shows fast temporal response and excellent reversibility due to being without parasitic electrical effects and flexible packaging. As a proof-of-concept application, wrist pulse waveforms together with skin temperature are recorded simultaneously, which is critical to the cardiovascular problem analysis. Owing to the seamless connection with standard optical fiber, we believe our sensor is especially useful in healthcare, robotics, and human–machine interface applications.

**Disclosures.** The authors declare no conflicts of interest.

**Data Availability.** The data that support the findings of this study are available from the corresponding authors upon reasonable request.

†These authors contributed equally to this paper.

## REFERENCES

1. K. Song, R. D. Zhao, Z. L. Wang, and Y. Yang, "Conjuncted pyro-piezoelectric effect for self-powered simultaneous temperature and pressure sensing," Adv. Mater. **31**, 1902831 (2019).
2. S. B. Han, N. U. A. Alvi, L. Granlof, H. Granberg, M. Berggren, S. Fabiano, and X. Crispin, "A multiparameter pressure-temperature-humidity sensor based on mixed ionic-electronic cellulose aerogels," Adv. Sci. **6**, 1802128 (2019).
3. F. C. Li, Y. Liu, X. L. Shi, H. P. Li, C. H. Wang, Q. Zhang, R. J. Ma, and J. J. Liang, "Printable and stretchable temperature-strain dual-sensing nanocomposite with high sensitivity and perfect stimulus discriminability," Nano Lett. **20**, 6176–6184 (2020).
4. J. Kim, A. S. Campbell, B. E.-F. de Ávila, and J. Wang, "Wearable biosensors for healthcare monitoring," Nat. Biotechnol. **37**, 389–406 (2019).
5. J. Shin, Z. H. Liu, W. B. Bai, Y. H. Liu, Y. Yan, Y. G. Xue, I. Kandela, M. Pezhouh, M. R. MacEwan, Y. G. Huang, W. Z. Ray, W. D. Zhou, and J. A. Rogers, "Bioresorbable optical sensor systems for monitoring of intracranial pressure and temperature," Sci. Adv. **5**, eaaw1899 (2019).
6. A. Leal-Junior, J. J. Guo, R. Min, A. J. Fernandes, A. Frizera, and C. Marques, "Photonic smart bandage for wound healing assessment," Photonics Res. **9**, 272–280 (2021).
7. J. C. Yang, J. Mun, S. Y. Kwon, S. Park, Z. N. Bao, and S. Park, "Electronic skin: recent progress and future prospects for skin-attachable devices for health monitoring, robotics, and prosthetics," Adv. Mater. **31**, 1904765 (2019).
8. C. Zhang, S. Liu, X. Huang, W. Guo, Y. Li, and H. Wu, "A stretchable dual-mode sensor array for multifunctional robotic electronic skin," Nano Energy **62**, 164–170 (2019).
9. K. Sim, Z. Y. Rao, Z. N. Zou, F. Ershad, J. M. Lei, A. Thukral, J. Chen, Q.-A. Huang, J. L. Xiao, and C. J. Yu, "Metal oxide semiconductor nanomembrane–based soft unnoticeable multifunctional electronics for wearable human-machine interfaces," Sci. Adv. **5**, eaav9653 (2019).
10. M. Wang, T. Wang, Y. F. Luo, K. He, L. Pan, Z. Li, Z. Q. Cui, Z. H. Liu, J. Q. Tu, and X. Chen, "Fusing stretchable sensing technology with machine learning for human-machine interfaces," Adv. Funct. Mater. **31**, 2008807 (2021).
11. Q. L. Hua, J. L. Sun, H. T. Liu, R. R. Bao, R. M. Yu, J. Y. Zhai, C. F. Pan, and Z. L. Wang, "Skin-inspired highly stretchable and conformable matrix networks for multifunctional sensing," Nat. Commun. **9**, 244 (2018).
12. J. X. Chen, H. J. Wen, G. L. Zhang, F. Lei, Q. Feng, Y. Liu, X. D. Cao, and H. Bong, "Multifunctional conductive hydrogel/thermochromic elastomer hybrid fibers with a core-shell segmental configuration for wearable strain and temperature sensors," ACS Appl. Mater. Interfaces **12**, 7565–7574 (2020).
13. J. H. Rao, Z. T. Chen, D. N. Zhao, R. Ma, W. Y. Yi, C. X. Zhang, D. Liu, X. Chen, Y. H. Yang, X. F. Wang, J. Wang, Y. J. Yin, X. F. Wang, G. W. Yang, and F. Yi, "Tactile electronic skin to simultaneously detect and distinguish between temperature and pressure based on a triboelectric nanogenerator," Nano Energy **75**, 105073 (2020).
14. K. Dong, X. Peng, and Z. L. Wang, "Fiber/fabric-based piezoelectric and triboelectric nanogenerators for flexible/stretchable and wearable electronics and artificial intelligence," Adv. Mater. **32**, 1902549 (2020).
15. A. Chhetry, S. Sharma, S. C. Barman, H. Yoon, S. Ko, C. Park, S. Yoon, H. Kim, and J. Y. Park, "Black phosphorus@laser-engraved graphene heterostructure-based temperature-strain hybridized sensor for electronic-skin applications," Adv. Funct. Mater. **31**, 2007661 (2021).
16. B. Lee, "Review of the present status of optical fiber sensors," Opt. Fiber Technol. **9**, 57–79 (2003).
17. H. C. Zhao, K. O'Brien, S. Li, and R. F. Shepherd, "Optoelectronically innervated soft prosthetic hand via stretchable optical waveguides," Sci. Robot. **1**, eaai7529 (2016).
18. S. M. Wang, X. L. Ni, L. Y. Li, J. Y. Wang, Q. Liu, Z. J. Yan, L. Zhang, and Q. Z. Sun, "Noninvasive monitoring of vital signs based on highly sensitive fiber optic mattress," IEEE Sens. J. **20**, 6182–6190 (2020).

19. J. J. Guo, B. Q. Zhou, C. X. Yang, Q. H. Dai, and L. J. Kong, "Stretchable and upconversion-luminescent polymeric optical sensor for wearable multifunctional sensing," Opt. Lett. **44**, 5747–5750 (2019).

20. J. T. Zhou, C. R. Liao, Y. P. Wang, G. L. Yin, X. Y. Zhong, K. M. Yang, B. Sun, G. J. Wang, and Z. Y. Li, "Simultaneous measurement of strain and temperature by employing fiber Mach-Zehnder interferometer," Opt. Express **22**, 1680–1686 (2014).

21. C. P. Lin, Y. Wang, Y. J. Huang, C. R. Liao, Z. Y. Bai, M. X. Hou, Z. Y. Li, and Y. P. Wang, "Liquid modified photonic crystal fiber for simultaneous temperature and strain measurement," Photonics Res. **5**, 129–133 (2017).

22. A. Leal-Junior, A. Frizera, H. Lee, Y. Mizuno, K. Nakamura, T. Paixao, C. Leitao, M. F. Domingues, N. Alberto, P. Antunes, P. Andre, C. Marques, and M. J. Pontes, "Strain, temperature, moisture, and transverse force sensing using fused polymer optical fibers," Opt. Express **26**, 12939–12947 (2018).

23. C. L. Fu, Y. P. Wang, S. Liu, Z. Y. Bai, J. Tang, L. P. Shao, and X. Y. Liu, "Transverse-load, strain, temperature, and torsion sensors based on a helical photonic crystal fiber," Opt. Lett. **44**, 1984–1987 (2019).

24. Y. Y. Zhi, X. Li, Y. P. Li, J. Li, and B.-O. Guan, "Superstructure microfiber grating characterized by temperature, strain, and refractive index sensing," Opt. Express **28**, 8853–8861 (2020).

25. L. M. Tong, R. R. Gattass, J. B. Ashcom, S. L. He, J. Y. Lou, M. Y. Shen, I. Maxwell, and E. Mazur, "Subwavelength-diameter silica wires for low-loss optical wave guiding," Nature **426**, 816–819 (2003).

26. L. M. Tong, J. Y. Lou, and E. Mazur, "Single-mode guiding properties of subwavelength-diameter silica and silicon wire waveguides," Opt. Express **12**, 1025–1035 (2004).

27. L. Zhang, Y. Tang, and L. M. Tong, "Micro-/nanofiber optics: merging photonics and material science on nanoscale for advanced sensing technology," iScience **23**, 100810 (2020).

28. J. Li, J. Chen, and F. Xu, "Sensitive and wearable optical microfiber sensor for human health monitoring," Adv. Mater. Technol. **3**, 1800296 (2018).

29. H.-T. Zhu, L.-W. Zhan, Q. Dai, B. Xu, Y. Chen, Y.-Q. Lu, and F. Xu, "Self-assembled wavy optical microfiber for stretchable wearable sensor," Adv. Opt. Mater. **9**, 2002206 (2021).

30. L. Y. Li, Y. F. Liu, C. Y. Song, S. F. Sheng, L. Y. Yang, Z. J. Yan, D. J. J. Hu, and Q. Z. Sun, "Wearable alignment-free microfiber-based sensor chip for precise vital signs monitoring and cardiovascular assessment," Adv. Fiber Mater. **4**, 475–486 (2022).

31. Y. P. Li, S. J. Tan, L. Y. Yang, L. Y. Li, F. Fang, and Q. Z. Sun, "Optical microfiber neuron for finger motion perception," Adv. Fiber Mater. **4**, 226–234 (2022).

32. J. Pan, Z. Zhang, C. P. Jiang, L. Zhang, and L. M. Tong, "A multifunctional skin-like wearable optical sensor based on an optical micro-/nanofibre," Nanoscale **12**, 17538–17544 (2020).

33. L. Zhang, J. Pan, Z. Zhang, H. Wu, N. Yao, D. W. Cai, Y. X. Xu, J. Zhang, G. F. Sun, L. Q. Wang, W. D. Geng, W. G. Jin, W. Fang, D. W. Di, and L. M. Tong, "Ultrasensitive skin-like wearable optical sensors based on glass micro/nanofibers," Opto-Electron. Adv. **3**, 190022 (2020).

34. Y. Tang, H. T. Liu, N. Yao, Z. Zhang, Y. Xu, N. Yao, L. Zhang, and L. M. Tong, "Optical micro/nanofiber-enabled compact tactile sensor for hardness discrimination," ACS Appl. Mater. Interfaces **13**, 4560–4566 (2021).

35. R. S. Johansson and A. B. Vallbo, "Detection of tactile stimuli. Thresholds of afferent units related to psychophysical thresholds in the human hand," J. Physiol. **297**, 405–422 (1979).

36. I. You, D. G. Mackanic, N. Matsuhisa, J. Kang, J. Kwon, L. Beker, J. Mun, W. Suh, T. Y. Kim, J. B. H. Tok, Z. Bao, and U. Jeong, "Artificial multimodal receptors based on ion relaxation dynamics," Science **370**, 961–965 (2020).

37. Y. Lee, J. Park, A. Choe, S. Cho, J. Kim, and H. Ko, "Mimicking human and biological skins for multifunctional skin electronics," Adv. Funct. Mater. **30**, 1904523 (2020).

38. E. Udd, *Fiber Optic Sensors: An Introduction for Engineers and Scientists* (Wiley, 1991).

39. C. H. Dong, L. He, Y. F. Xiao, V. R. Gaddam, S. K. Ozdemir, Z. F. Han, G. C. Guo, and L. Yang, "Fabrication of high-Q polydimethylsiloxane optical microspheres for thermal sensing," Appl. Phys. Lett. **94**, 231119 (2009).

40. J. N. Cohn, S. Finkelstein, G. McVeigh, D. Morgan, L. LeMay, J. Robinson, and J. Mock, "Noninvasive pulse wave analysis for the early detection of vascular disease," Hyperension **26**, 503–508 (1995).

41. J. Park, M. Kim, Y. Lee, H. S. Lee, and H. Ko, "Fingertip skin-inspired microstructured ferroelectric skins discriminate static/dynamic pressure and temperature stimuli," Sci. Adv. **1**, e1500661 (2015).